Geophysical Research Letters

RESEARCH LETTER
10.1029/2018GL079684

Key Points:
- Unexpected increases in the global phytoplankton biomass
- Phytoplankton biomass in tropics is driven by El Niño–Southern Oscillation

Supporting Information:
- Supporting Information S1
- Figure S1
- Figure S2
- Figure S3
- Figure S4
- Figure S5
- Figure S6
- Figure S7
- Figure S8
- Figure S9
- Figure S10
- Figure S11
- Figure S12
- Figure S13

Correspondence to:
P. Sharma,
priyash@sas.upenn.edu

Citation:
Sharma, P., Marinov, I., Cabre, A., Kostadinov, T., & Singh, A. (2019). Increasing biomass in the warm oceans: Unexpected new insights from SeaWiFS. *Geophysical Research Letters*, *46*. https://doi.org/10.1029/2018GL079684

Received 19 JUL 2018
Accepted 11 MAR 2019
Accepted article online 18 MAR 2019

Increasing Biomass in the Warm Oceans: Unexpected New Insights From SeaWiFS

P. Sharma[1,2], I. Marinov[1], A. Cabre[3], T. Kostadinov[4], and A. Singh[2]

[1]Department of Earth and Environmental Science, University of Pennsylvania, Philadelphia, Pennsylvania, USA, [2]Pacific Center of Environment and Sustainable Development, The University of the South Pacific, Suva, Fiji, [3]Department of Physical Oceanography, Institute of Marine Sciences, CSIC, Barcelona, Spain, [4]Department of Liberal Studies, California State University San Marcos, San Marcos, California, USA

Abstract Marine phytoplankton biomass and community structure are expected to change under global warming, with potentially significant impacts on ocean carbon, nutrient cycling, and marine food webs. Previous studies have indicated decreases of primary production and chlorophyll *a* concentrations and oligotrophic gyre expansions from satellite ocean-color measurements, purportedly due to global warming. We review this topic via a reanalysis of a novel backscattering-based phytoplankton functional type and phytoplankton biomass time series over the 1997–2010 period. Unlike previous work, we find that globally the biomass and the percent of large (small) phytoplankton increase (decrease). The oligotrophic gyres contract or expand depending on the chlorophyll *a* threshold definition employed. In the subtropical gyres, chlorophyll *a* trends are likely due to physiological changes, while the increasing biomass trends are due to winds and relevant mixing length scale increases.

1. Introduction

Oxygenic photosynthesis by phytoplankton contributes to nearly half of the biosphere's net primary production (Field et al., 1998). The density contrast between the surface layer and underlying cooler nutrient-rich waters below the permanent pycnocline is expected to increase with a warmer ocean surface (Capotondi et al., 2012). This enhanced stratification will likely reduce nutrient supply to the surface and decrease ocean biological productivity differentially across biomes (Behrenfeld et al., 2006). It also will affect the biological pump, which effectively sequesters carbon away from the atmosphere for centuries to millennia (Eppley & Peterson, 1979). It is then crucial to understand any changes in phytoplankton biomass and size structure, as picophytoplankton typically outcompetes microphytoplankton in nutrient-poor environments (e.g., Weber & Deutsch, 2010).

Traditionally, satellite-based chlorophyll *a* (Chl *a*) has been used to assess the spatial distribution and temporal evolution of phytoplankton abundance and productivity (Behrenfeld et al., 2002; Boyce et al., 2010). No significant global temporal trends in Chl *a* were found using single ocean color satellite missions that span ~10 years (Beaulieu et al., 2013; Gregg, 2005; Gregg et al., 2003; Gregg & Rousseaux, 2014; Henson et al., 2010; Polovina et al., 2008; Siegel et al., 2013; Vantrepotte & Mélin, 2011). Gregg et al. (2017) recently used a new satellite merged 18-year time series and found no significant trend in global annual median Chl *a* from 1998 to 2015. Wernand et al. (2013) reconstructed Chl *a* changes from Forel-Ule scale records for the century-long 1889–2000 period and found compensating Chl *a* trends in different ocean regions.

Little work has been done on looking for trends in satellite-derived phytoplankton biomass (Behrenfeld et al., 2006) and community size structure (Kostadinov et al., 2010). Here we add to the subject by studying trends and interannual variability in the novel backscattering-based phytoplankton functional type (PFT)-partitioned phytoplankton biomass (Kostadinov et al., 2009, 2010, 2016), and comparing to Chl *a* over the 1997–2010 SeaWiFS (Sea-Viewing Wide Field-of-View Sensor) period. Our objective is to explore the underlying physical mechanisms responsible for observed biological trends across the warm regions (region with average sea surface temperature (SST) > 15 °C that includes tropical and subtropical biomes).

2. Data and Methods

We study the biological long-term trends and interannual variability in the warm oceans (region with average SST > 15 °C that includes tropical and subtropical biomes; Figure S1). We use a 9-km backscattering-

based particle size distribution phytoplankton biomass in mg m^{-3}, PFT biomass fractions expressed in percent [picoplankton (0.5–2-μm diameter), nanoplankton (2–20 μm), and microplankton (20–50 μm), hereafter micro%, nano%, and pico% as in Kostadinov et al. (2016), and 9 km Chl *a* (OCI (R2014))] for the SeaWiFS period 1997–2010. We derive a photoacclimation parameter (hereafter Chl/C_{B16}) based on Behrenfeld et al. (2016) (Text S1). We derive the active mixing length scale (L_{MIX}) for phytoplankton (Brody & Lozier, 2014, 2015), and the mixed layer depth (de Boyer Montégut et al., 2004). Other variables used are sea surface temperature (SST), 10-m wind speed (Berrisford et al., 2011), air-sea heat flux (positive into the ocean), photosynthetically available radiation (PAR), diffuse attenuation coefficient for downwelling irradiance at 490 nm ($K_d(490)$), and particulate inorganic carbon (PIC). Texts S1 and S2 provide details on data sources and definitions. High-resolution variables are downsampled to a 1° grid using a 12 × 12 top-hat averaging kernel. If >50% of the pixels being averaged are invalid data, the pixel is assigned a missing data value (as in Kostadinov et al., 2017). All monthly time resolution data sets are used. All anomalies are relative to the 1998–2010 mean seasonal cycle, unless stated otherwise. We use generalized least squares regression to calculate temporal trends in variables (as in Beaulieu et al., 2013) and present the uncertainty at the 68% confidence level (~0.3 *p* value) unless stated otherwise. A Monte Carlo-based error analysis (Figure S13 and Text S4) confirms that trends are meaningful or significant at the 68% confidence interval. Note that significant here means that the 68% confidence interval (unless stated otherwise) of the slope of the generalized least squares regression of the monthly anomalies on time in years does not cross the zero line. Text S3 further separates the El Niño–Southern Oscillation (ENSO) and non-ENSO trend components, confirming the significance of our results and confidence analysis.

3. Global Trends in Biomass and Chl *a*

The 1997–2010 trends in total phytoplankton biomass are found to be significantly positive over most of the global ocean (Figure 1a and Table S1). Weak but significant negative trends (−0.5 to −1%/year) are only found along the equatorial and subtropical east Atlantic and off the west coast of Africa. Similar significant positive trends are observed for the micro% and nano% (Figures 1d and 1e). In contrast, the pico% (Figure 1f) shows negative trends globally.

The spatial trends in Chl *a* (Figure 1b) are comparable to those in Siegel et al. (2013, their Figure 4b). In cold regions (approximately north of 40°N and south of 40°S; Figure S1), Chl *a* increase patterns are identical to those found in the biomass. In warm regions, however, there are prominent significant negative Chl *a* trends along the west coast of North Africa, the Indian and Pacific subtropical gyres, contrary to the positive trends in biomass. Similar declines in low-latitude Chl *a* have been observed in previous SeaWiFS-based studies over different periods (Gregg, 2005; Gregg & Rousseaux, 2014; Henson et al., 2010; Siegel et al., 2013; Vantrepotte & Mélin, 2011). In warm regions, competing positive and negative trends in Chl *a* cancel out (Figure 1b); hence, the significant positive global trend is dominated by basin-wide increases in Chl *a* within the cold regions (Table S1). In contrast to Chl *a*, significant positive trends are found for biomass in the warm region and the cold regions.

How much of the biological trends in Figure 1 are ENSO driven? In most of the subtropics and subpolar regions, the positive non-ENSO trend in biomass dominates over the negative ENSO biomass trend, showing an overall global significant positive trend (see Text S3 and Figures S3 and S4). In the tropical Pacific tongue, the strong positive trends in biomass and Chl *a* are due to the added effects of the strong positive ENSO trend and a weak positive non-ENSO trend.

The warm and cold SH regions individually explain 44% and 46% of the global biomass increase in Figure 1 (Table S1 and Text S3). We focus here on understanding the warm region trends. The tropical Pacific tongue and the subtropical gyres explain 33% and 21% of the warm biomass trends, respectively.

4. ENSO Impacts on Phytoplankton Biomass and PFTs in the Tropical Pacific

El Niño–Southern Oscillation (ENSO) is the strongest global climate natural fluctuation on interannual time scales, with a warm (El Niño) and a cold (La Niña) phase. Sustained El Niño phase generates long-lasting positive SST anomalies across the equatorial Pacific basin associated with weaker-than-average trade winds, an eastward expansion of the warm pool leading to increased water stratification in the east, a flattening of

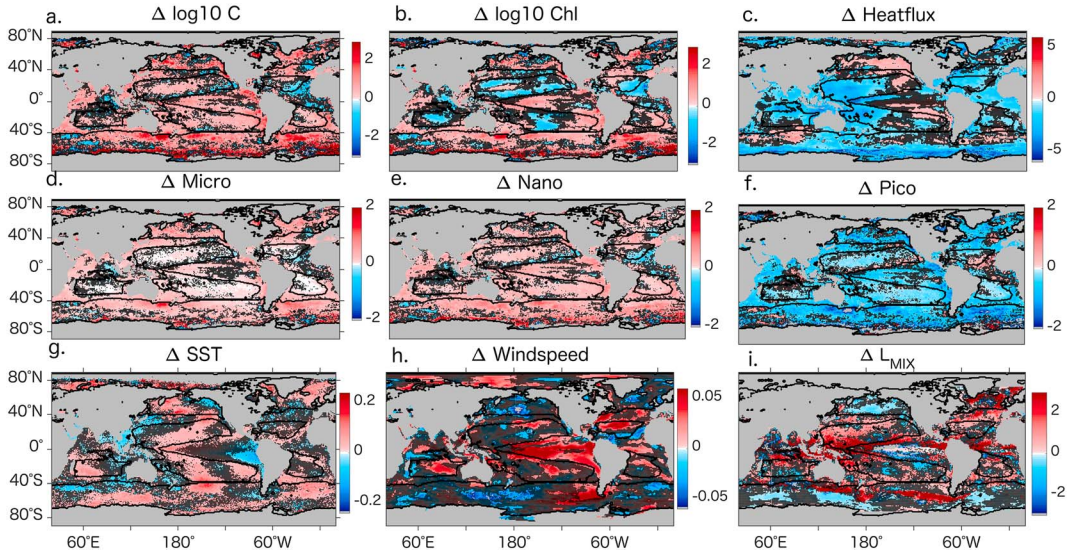

Figure 1. GLS trends for deseasonalized monthly anomalies of SeaWiFS-derived (a) phytoplankton biomass concentration, (b) Chl *a* concentration, (d) fraction microphytoplankton, (e) fraction nanophytoplankton, and (f) fraction picophytoplankton, all in %/year. Linear trends in (c) heat flux (Wm^{-2}/year), (g) SST (°C/year), (h) wind speed (ms^{-1}/year), and (i) L_{MIX} (m/year). All trends are for the 1997–2010 period. Pixels with statistically insignificant trends at the 68% confidence interval ($p < 0.3$) are hatched. Biomes are (Figure S1) delimited by black contours.

the thermocline/nutricline (Chavez et al., 1998; Christian et al., 2001; Radenac et al., 2001; Stone et al., 1999; Strutton & Chavez, 2000; Turk et al., 2001), and decrease in phytoplankton growth along most of the tropical Pacific cold tongue except in the western region where phytoplankton increases (Radenac et al., 2012).

We find that most interannual variability in phytoplankton biomass and Chl *a* is associated with ENSO in the tropical Pacific tongue, as indicated by significant negative correlations between the multivariate ENSO index (MEI) and the analyzed variables (Figure 2a and Table S2). During La Niña (negative MEI), strong westward trade winds shoal the eastern Pacific nutricline and increase both vertical nutrient supply to the surface and westward lateral nutrient inputs from the eastern equatorial Pacific, increasing biomass, Chl *a*, micro%, and nano%, and decreasing pico% (Figure 2b). The opposite happens during El Niño.

During our study period, a decreasing trend in MEI followed by an increasing trend (with a time split at 2002) was found to be significant at 95% confidence interval and more meaningful than a simple single linear trend (Figure 2a). The preferred time split was found by performing two separate linear regressions on MEI from 1999 to the split time and from the split time to the end (2010) for every possible split time (as in Beaulieu et al., 2012). Biomass and Chl *a* first decrease during 1999–2002, when the MEI time series is increasing (hereafter, "El Niño"-like state) and then increases when the MEI is decreasing (hereafter, "La Niña"-like state) during 2002–2010. The trend over the full SeaWiFS period is dominated by the transition from the large 1997–98 El Niño event to the increasingly negative MEI period of 2002–2010, and corresponds to an increase in tropical Pacific biomass and Chl *a* (compare Figure 2b with Figures 1a, 1b, and 1d).

5. Variability/Trends in Carbon Biomass in the Subtropical Gyres

Global warming is expected to further stratify the subtropical gyres (Polovina et al., 2011). With decreased nutrient supply to the surface oligotrophic ocean, the phytoplankton biomass will likely decrease (Behrenfeld et al., 2006; Boyce et al., 2010) and shift from large- to small-sized species (Bopp et al., 2005; Boyd & Doney, 2002; Corno et al., 2007). We show here results contrary to this hypothesis. The 1997–2010 period is dominated by declines in the pico% and increases in the micro%, nano%, and biomass in the subtropical gyres, significant everywhere except for the North Atlantic Gyre (NATL; Table S3). Most of the error bars do not cross the horizontal and vertical zero line in Figure S13, which indicates that most of the PFTs and biomass are significant at 68% confidence interval. We note that biomass and micro%/nano% is not

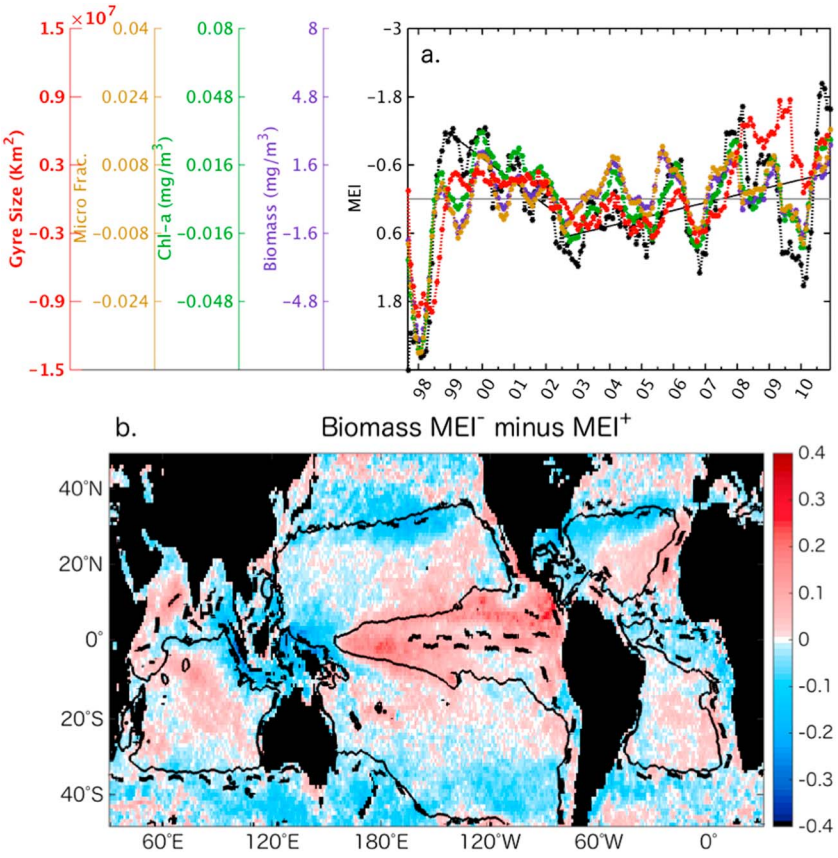

Figure 2. (a) Time series of deseasonalized anomalies of tropical Pacific tongue biomass, microfraction, Chl *a*, gyre size, and the MEI index. Note that the *y* axis of MEI time series is reversed (black). (b) Difference in biomass anomalies during large negative (> −1, red, during cold phase) and positive phases (< +1, blue, during warm phase) of the MEI. The black solid and dashed lines is the Chl *a* contour at 0.11 mg/m^3 during large negative MEI and positive MEI, respectively.

significantly correlated with MEI in the subtropical gyres (Table S3). What could then drive the observed biomass increases?

Following up on recent efforts (Brody & Lozier, 2014, 2015), we derive a phytoplankton active mixing length scale (L_{MIX}; details in Text S2) that accounts for mixing due to a large negative heat flux (out of the ocean) generating deep convective mixing to the base of the seasonal pycnocline (L_{MIX} = MLD, Case 1), mixing proportional to wind energy ($L_{MIX} = L_{EK}$, Case 2), and reduced turbulent mixing when large positive heat flux (into the ocean) counteracts wind mixing ($L_{MIX} = L_{OZ}$, Case 3; Figure S5). The contribution of the various cases to L_{MIX} (meaning the percentage of pixels with one or the other case) is shown in Figure S12.

We find positive interannual correlations between L_{MIX} and biomass anomalies (Figure S6d) in the subtropical gyres, consistent with a deepening of the active mixing-length scale increasing vertical nutrient supply. Interannually, biomass is more tightly positively coupled to winds and L_{EK} in the subtropics than to MLD (Figures S6b–S6e). Heat flux into the ocean and biomass are negatively correlated (Figure S6c) across all gyres, indicating that as ocean heat uptake is weakening the biomass is increasing. The temporal correlation between monthly biomass and physical variables is weaker when seasonality is removed (not shown) compared to when the seasonality is included (Figure S6), as expected from other recent work (e.g., Dave & Lozier, 2010; Cabre et al., 2016).

We find that L_{MIX} increases in all the gyres where biomass increases significantly (except in NATL) throughout our study period (Table S1). We further analyze the monthly trends in biomass and physical drivers across all gyres.

In the North Pacific (NPAC) gyre, L_{MIX}/MLD/L_{EK} all peak in January/February when heat is lost from the ocean and the water column mixes deeply, bringing more nutrients to the surface and setting up the large

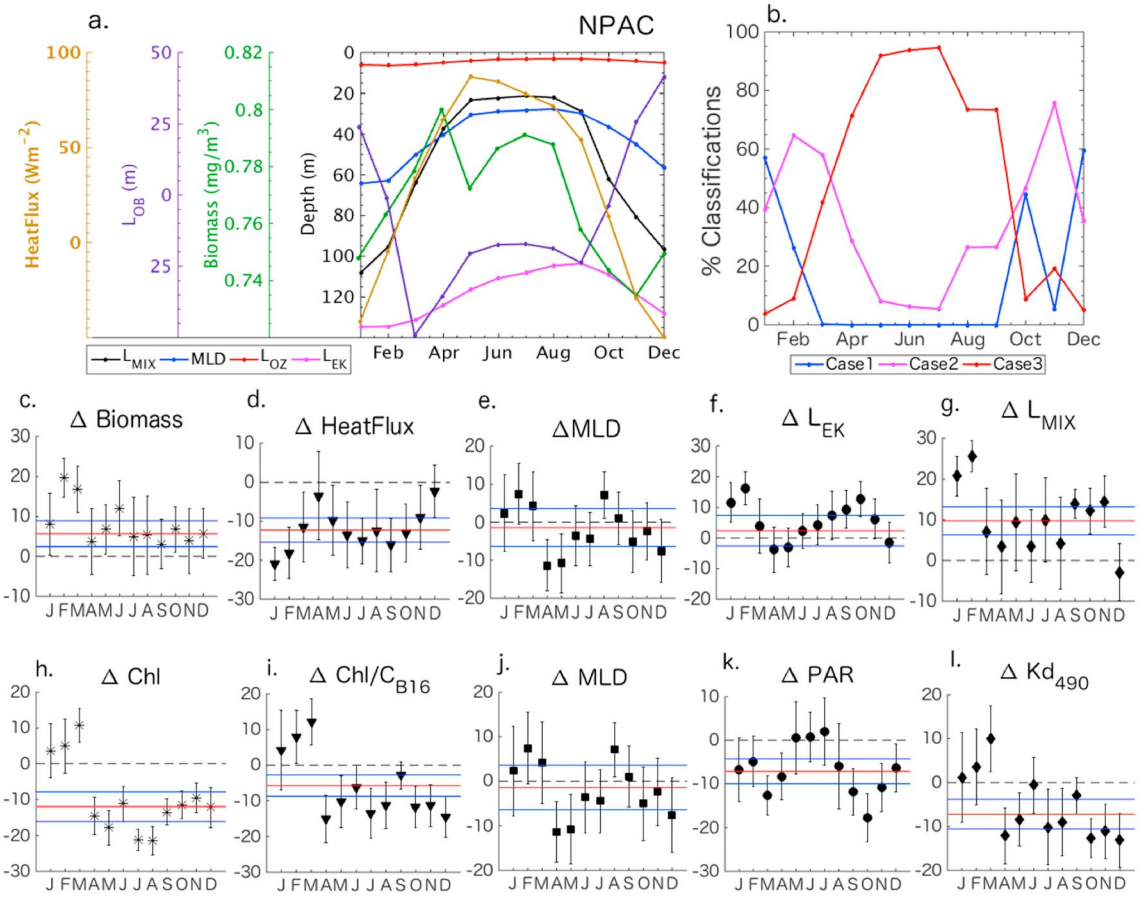

Figure 3. (a) The 1997–2010 averaged monthly climatology for L_{MIX} depth measurements for the NPAC with mixing depth measurements derived for all the Cases 1 (MLD), 2 (L_{EK}), and 3 (L_{OZ}) from surface atmospheric forcings. Log_{10} phytoplankton biomass and surface heat flux averaged monthly values are in green and gold. (b) The 1997–2010 averaged monthly climatology for percentage of pixels in the gyre that are classified as Case 1, 2, or 3 mixing. Percentage change/trends in all the months throughout 1997–2010 in the NPAC for the biome-averaged (c) biomass, (d) heat flux, (e) MLD, (f) L_{EK}, (g) L_{MIX}, (h) Chl *a*, (i) Chl/C_{B16}, (j) MLD, (k) PAR, and (l) $K_d(490)$. The red line is the total percentage change of biomass over the 1997–2010 period and the blue line is the ±1-sigma error (or 68% confidence interval, $p < 0.3$) associated with the total percentage change of biomass.

April biomass bloom (Figure 3a). A secondary biomass bloom is in July/August. In this gyre, both biomass and L_{MIX} increase every month of the year over the 1997–2010 period. The highest increase in biomass is in late winter/early spring (February–March) and is explained by increased February ocean heat loss, decreased March ocean heat uptake, and wind-driven L_{MIX} (Figures 3c–3g and S5). Note that 1-sigma error bars do not cross zero line, indicating that the trends are significant at 68% confidence interval for the winter months.

NATL gyre biomass peaks in July/August; a secondary biomass peak in January/February/March corresponds to strong winds and ocean heat loss driving maxima in MLD/L_{EK}/L_{MIX} (Figure S8). Over the period studied, we find the largest increase in biomass in February/March, corresponding to intensified heat flux loss and L_{MIX} (February/March), and increased MLD (January/February; Figures S8c–S8g). The largest drop occurs during April, corresponding to enhanced stratification, a shift to more (less) frequent Case 3 (Case 2) mixing and hence L_{MIX} decrease. Overall, monthly trends cancel each other, resulting in a weak negative but insignificant biomass trend.

The South Pacific (SPAC) gyre biomass (Figure S9a) shows one major peak in winter (June/July/August). Biomass increases significantly over 1997–2010 in all months. We propose that a combination of ocean heat flux loss (significant trends 8 months/year), increased winds (and L_{EK}, June–December), MLD (July–November), and L_{MIX} (August–January) contribute to the biomass growth in this domain (Figures S9c–S9g). The largest increase in the major seasonal peak of biomass (June-July-August)

corresponds to stronger winds, reduced ocean heat flux uptake (in June/August), and an increase in August L_{MIX} (likely driven by a shift from Case 3 to Case 1).

In the South Atlantic (SATL) subtropical gyre we see a single biomass peak in wintertime (June/July/August), when heat flux is at its most negative, and L_{MIX}/MLD/L_{EK} all peak together. An increase in annually averaged biomass is driven by increases in five months of the year (Figure S10c). Most increase in biomass is in May-June-July and can only be partially explained by a significant decrease in heat flux in May–June, a significant increase in MLD in June–July and a significant increase in L_{MIX} in May and July (Figures S10c–S10g).

The major peak in Indian (IOCE) gyre biomass is in June/July/August, corresponding to the period of maximum heat flux loss and both deepest MLD and strongest winds. The increase in biomass in the IOCE is largest in May/June/July when L_{MIX} is given by a combination of MLD and L_{EK} (Figures S11c–S11g). We partially ascribe the early winter increase in biomass to a significant increase in MLD and L_{MIX} in April/May/June, combined with wind increases (May–August).

In addition to the discussed bottom-up effects (increased nutrient supply), it is possible for increases in L_{MIX} to increase phytoplankton biomass via top-down effects. If deeper L_{MIX} dilutes zooplankton more than phytoplankton (Boss and Behrenfeld, 2010), this gives phytoplankton a boost as grazing pressure is reduced. Additionally, observed SST increases directly contribute to the increase in phytoplankton growth but also intensify zooplankton growth and grazing pressure. In the absence of global zooplankton data time series, it is challenging to clarify the potential contribution from a top-down mechanism.

In summary, we can partially ascribe the 1997–2010 increase in subtropical gyre biomass and a community shift toward more micro/nano% (less pico%) to an increased nutrient renewal during winter, as MLD and/or L_{MIX} increase by enhanced wind mixing and wintertime ocean heat loss (deeper convective mixing to the base of the permanent pycnocline). The contribution of Cases 1–3 to the average L_{MIX} seasonal cycle and the changes in these cases are detailed in Figure S12. The year-averaged contribution of Case 1 and 2 L_{MIX} into each subtropical gyre L_{MIX} increase for all the gyres, while Case 3 L_{MIX} decreases for most of the gyres (Table S4), as L_{MIX} increases during winter but remains approximately constant throughout the rest of the year. However, these changes are not significant, which suggests that the different mixing contributions remain approximately constant throughout our 1997–2010. Wintertime trends in L_{MIX} and biomass seem better coupled in some gyres (e.g., NPAC) but more decoupled in others (e.g., SATL).

It is known that increased carbon dioxide (CO_2) in surface water decreases the pH (increased ocean acidification) and causes calcareous organisms to dissolve (Doney et al., 2009; Mackey et al., 2015). However, some studies report that an elevated CO_2 favors photosynthesis in coccolithophores (which belong to the nano-phytoplankton group), thus increasing or restoring their calcification after an adaptation period (Iglesias-Rodriguez et al., 2008; Krumhardt et al., 2016; Schluter et al., 2014). Some recent studies have noticed coccolithophore abundance increase in response to surface partial pressure of carbon dioxide ($spCO_2$) increase (Krumhardt et al., 2016; Rivero-Calle et al., 2015). Rivero-Calle et al. (2015) claim that North Atlantic coccolithophore abundance increased from 2 to 20% from 1965 to 2010. In our study, we find increases in $spCO_2$ and nano% trends for all gyres (Table S3). Satellite-derived PIC (coccolithophores proxy) trends are positive only in the SATL and NATL gyres (Table S3). We posit that increasing trends in $spCO_2$ contributed to increased coccolithophore presence in the NATL and SATL gyres, consistent with increases in PIC and nano%.

6. Decoupling Between Biomass and Chl *a* in Subtropical Gyres

A major finding is the strong decoupling between Chl *a* and biomass trends (Figures 1a and 1e) in the subtropical gyres. Overall, we find increases in biomass in all the gyres over the 1997–2010 period and decreases in Chl *a* in three of the gyres (NPAC, NATL, IOCE). Why are biomass and Chl decoupled? First, ocean color can only sample the few upper meters of the water column, above the deep chlorophyll maximum conditions (Volpe et al., 2012). Thus, part of the phytoplankton vertical distribution is undetected by satellites that explain the extremely oligotrophic character that gyres display when sampled via remote sensing (Volpe et al., 2007). Second, the photoacclimation process, known to be dominant in the subtropics (e.g., Barbieux et al., 2018; Siegel et al., 2013), introduces variability in Chl *a* uncoupled from the biomass.

Although the large-scale, climatological distribution of Chl *a* largely reflects patterns in nutrient supply and thereby differences in phytoplankton abundances (Figures S2a and S2b), changes in light and nutrients can result in changes in pigment composition (Chl *a*; Rodríguez et al., 2006) not necessarily associated with biomass changes (Behrenfeld et al., 2002; Behrenfeld et al., 2005; Behrenfeld et al., 2016; Laws & Bannister, 1980; Paasche, 1998). Phytoplankton photoacclimate by adjusting their photosynthetic pigment (Chl *a*), such that a decrease in Chl/C_{B16} and Chl *a* may be due to (1) increase in surface light availability (PAR), (2) increase in light penetration in the water column (decrease in $K_d(490)$), or (3) shoaling of MLD, trapping plankton in the highly lit surface layer (Westberry et al., 2016).

Throughout the analyzed SeaWiFS period, trends in Chl/C_{B16} are consistent in sign with trends in Chl *a* in all the subtropical gyres. These trends are negative in the NPAC, NATL, and IOCE (insignificant in IOCE) and positive in the SPAC and SATL (Table S3). We further analyze the monthly trends to explain Chl *a* and Chl/C_{B16} trends.

The Chl *a* peaks (lowest) in winter, December–February (September–October) for NPAC, when the MLD is deeper (shallow), PAR is lowest (highest) and light penetration is weakest, $K_d(490)$ maxima (strongest, $K_d(490)$ minimum). Over the period we find that the significant MLD shoaling, and $K_d(490)$ decrease in the NPAC gyre, drives Chl *a* decrease from April to December (Figures S3h–S3l). The changes in biomass and Chl *a* are coupled in late winter and spring, but decoupled during the summer months. In NATL, Chl *a* also peaks in winter months and is lowest from April to June. A significant decrease $K_d(490)$ in the NATL gyre drives Chl *a* to decrease (especially April–June; Figures S6h–S6l). The biomass and Chl *a* changes are decoupled over the period in NATL gyre. In both NPAC and NATL, Chl/C_{B16} decreases as cells acclimate to the increased exposure to light (Table S3) during summer months.

For the gyres in the Southern Hemispheres, the Chl *a* is maximum during the winter months (June-to-August), when the MLD is deeper, PAR is lowest, and $K_d(490)$ at maxima. The combination of year-averaged MLD shoaling, $K_d(490)$ decrease, and PAR increase that is observed in the IOCE could be driving the small decrease in Chl/C_{B16}. A significant MLD shoaling and $K_d(490)$ decrease drive Chl *a* and Chl/C_{B16} decrease from January to April, and increase in $K_d(490)$ from May to August control the increase in Chl/C_{B16} (Figures S11h–S11l). Both biomass and Chl *a* are changes are coupled and driven by MLD deepening throughout the period.

In contrast, year-averaged MLD deepening and $K_d(490)$ increase cause a small Chl/C_{B16} increase in the SPAC and SATL. The significant MLD deepening and $K_d(490)$ increase in SPAC are mostly observed during July–November, that is consistent with Chl *a* increase. The significant MLD deepening and $K_d(490)$ increase in SATL for July–August explain the increase in Chl/C_{B16} and Chl *a*. We also note that the biomass and Chl *a* are coupled in both the gyres, commonly driven by the deepening of MLD (Figures S10 and S11h–S11l).

We also found that Chl *a* and Chl/C_{B16} show a strong positive interannual correlation in the subtropical gyres while biomass and Chl/C_{B16} are weakly correlated. In agreement with recent work (Behrenfeld et al., 2016; Siegel et al., 2013; Westberry et al., 2016), we conclude that acclimation strongly impacts Chl/C_{B16} ratios and hypothesize that the above acclimation trends, rather than biomass trends, explain the 1997–2010 subtropical gyre Chl *a* trends.

We also note that the magnitude of the trends in Chl *a* has changed slightly from the standard (STD) algorithm (R2010) processing to the Ocean Color Index (OCI) algorithm processing (R2014); the globally averaged trends in Chl *a* became less negative/more positive (and more like our biomass) for the OCI. Signorini et al. (2015) analyzed trends in Chl *a* for both the STD and OCI algorithms for all subtropical gyres and also reported similar trends as our Chl *a* trends among the different sensors and algorithms, with small differences in the magnitude.

7. Trends in Gyre Sizes

Previous studies have claimed an increase in gyre size over recent decades corresponding to an expansion of the low Chl *a* core (Martinez et al., 2009). Polovina et al. (2008) concluded that the Pacific and Atlantic subtropical gyres are expanding at average annual rates from 0.8 to 4.3% throughout the 1998–2006

SeaWiFS period, and ascribed this to climate-driven increases in SST and vertical stratification. Irwin and Oliver (2009) reported expansion of the hyperoligotrophic subtropical gyres during the 1998–2007 period.

We find that the trends in gyre sizes depend on the considered Chl *a* threshold over the period 1997–2010 (Table S3). When using low thresholds, that is, Chl $a < 0.07$ mg/m^3, as in previous studies (McClain et al., 2004; Polovina et al., 2008; Signorini & McClain, 2012; Signorini et al., 2015), we find insignificant positive trends in three of the gyres, and significant negative trends in the SPAC and SATL gyres. When discussing the gyre size using higher thresholds (e.g., Chl $a < 0.11$ mg/m^3), the effect of ENSO becomes important. A negative MEI is associated with a broader Tropical Pacific tongue and smaller Pacific, Indian, and SATL gyres (Table S2). During the SeaWiFS period, we find decreases in the oligotrophic gyre sizes associated with the transition toward a La Niña state (see section 4 and Figure 2a) that causes the tropical biomes to expand and the subtropical gyres to shrink (Figure 2b, compare solid and dashed lines).

8. Summary and Conclusions

This paper examines the trends and interannual variability of new estimates of biomass and PFT fractions in comparison to changes in Chl *a* over the 1997–2010 period. We find a global increase in biomass, micro% and nano%. This increase differs from previous findings and is somewhat surprising given previously reported decreases in Chl *a* (previously used as a proxy of biomass) in the warm regions.

In the subtropical gyres, some previous literature claimed that increased stratification has already resulted in decreased phytoplankton abundance and primary production (Figure 3 of Behrenfeld et al., 2006; Figure 1 of Martinez et al., 2009) and an expansion of the low Chl *a* oligotrophic biome (Irwin & Oliver, 2009; Polovina et al., 2008). We find instead that over 1997–2010, biomass increases in all subtropical gyres while Chl *a* decreases in the NPAC, NATL, and IOCE gyres. We can partially ascribe the biomass increases to negative heat flux trends and stronger winds during winter deepening the L_{MIX}. Acidification-affected coccolithophore might also change biomass, particularly in the SATL. In contrast, we suggest that subtropical Chl *a* decreases are photoacclimation driven. Therefore, Chl *a* is not the best indicator for phytoplankton community structure and abundance.

In the tropical Pacific, we ascribe instead the observed increase in biomass over the 1997–2010 period to a trend toward a more La Niña-like state. Figure 2 confirms that the 1999–2004 Chl *a* and net primary production decrease reported for the warm ocean by Behrenfeld et al. (2006) is not a climate change signal as reported but a reflection of ENSO-driven variability in the tropical Pacific tongue. We also find that the oligotrophic gyres contract or expand depending on the Chl *a* threshold employed, and the 1997–2010 contraction of Chl $a < 0.11$ subtropical biomes is due to a slight trend toward more "La-Nina" conditions.

One caveat for this study is the relatively weak local interannual correlations between our various physical metrics and biomass (Figure S6), despite strong correlations on seasonal time scales (Cabre et al. 2016). This discrepancy has been recently discussed in other recent studies (e.g., Dave & Lozier, 2013; Lozier et al., 2011), suggesting that other factors not addressed here may play a role in the observed interannual correlations and trends, that is, advection of nutrients from the subpolar to the subtropical gyres, or mesoscale eddy dynamics (Ayers & Lozier, 2010; Dufois et al., 2016; Lehahn et al., 2017; Palter et al., 2005) and changes in the grazing pressure (Boss & Behrenfeld, 2010).

We cannot, at present, assign the biomass trends to climate-driven change, because of the short duration of ocean color satellite measurements. A reliable detection of trends would require a 20–30-year time series in the tropics and a 40-year time series elsewhere (Henson et al., 2010). Further merging of color products between various missions is critical for future clean separation of natural variability and climate-driven signals in ocean biology, with important ecological and biogeochemical impacts, as well as implications for fishery industries.

Acknowledgments
This work was supported by NASA grant NNX13AC92G to Marinov and Kostadinov. A. Cabre is grateful for the "Beatriu de Pinos" fellowship and the program Marie Curie Actions COFUND of the 7th Framework Program for Research and Technological Development of the European Union. We acknowledge research advice and conversations with L. Smith (Marine Ecosystem Dynamics Research Group, JAMSTEC, Japan) and S. Brody (McKinsey & Company). We thank Penn students Danica Fine and David Shields for the support in early stages of this work. Our phytoplankton biomass and PFT data are available at https://doi.pangaea.de/10.1594/PANGAEA.859005.

References

Ayers, J. M., & Lozier, M. S. (2010). Physical controls on the seasonal migration of the North Pacific transition zone chlorophyll front. *Journal of Geophysical Research*, *115*, C05001. https://doi.org/10.1029/2009JC005596

Barbieux, M., Uitz, J., Bricaud, A., Organelli, E., Poteau, A., Schmechtig, C., et al. (2018). Assessing the variability in the relationship between the particulate backscattering coefficient and the chlorophyll *a* concentration from a global biogeochemical-Argo database. *Journal of Geophysical Research: Oceans*, *123*, 1229–1250. https://doi.org/10.1002/2017JC013030

Beaulieu, C., Henson, S. A., Sarmiento, J. L., Dunne, J. P., Doney, S. C., Rykaczewski, R. R., & Bopp, L. (2013). Factors challenging our ability to detect long-term trends in ocean chlorophyll. *Biogeosciences*, *10*(4), 2711–2724. https://doi.org/10.5194/bg-10-2711-2013

Beaulieu, C., Sarmiento Jorge, L., Mikaloff Fletcher Sara, E., Chen, J., & Medvigy, D. (2012). Identification and characterization of abrupt changes in the land uptake of carbon. *Global Biogeochemical Cycles*, *26*, GB1007. https://doi.org/10.1029/2010GB004024

Behrenfeld, J. M., Emilio, M. Â., David, A. S., & Stanford, B. H. (2002). Photoacclimation and nutrient-based model of light-saturated photosynthesis for quantifying oceanic primary production. *Marine Ecology Progress Series*, *228*, 103–117. https://doi.org/10.3354/meps228103

Behrenfeld, M. J., Boss, E., Siegel, D. A., & Shea, D. M. (2005). Carbon-based ocean productivity and phytoplankton physiology from space. *Global Biogeochemical Cycles*, *19*, GB1006. https://doi.org/10.1029/2004GB002299

Behrenfeld, M. J., O'Malley, R. T., Boss, E. S., Westberry, T. K., Graff, J. R., Halsey, K. H., et al. (2016). Revaluating ocean warming impacts on global phytoplankton. *Nature Climate Change*, *6*(3), 323–330. https://doi.org/10.1038/nclimate2838. http://www.nature.com/nclimate/journal/v6/n3/abs/nclimate2838.html

Behrenfeld, M. J., O'Malley, R. T., Siegel, D. A., McClain, C. R., Sarmiento, J. L., Feldman, G. C., et al. (2006). Climate-driven trends in contemporary ocean productivity. *Nature*, *444*(7120), 752–755. https://doi.org/10.1038/nature05317

Berrisford, P., Dee, D., Poli, P., Brugge, R., Fielding, K., Fuentes, M., et al. (2011). The ERA-Interim archive version 2.0. Retrieved from

Bopp, L., Aumont, O., Cadule, P., Alvain, S., & Gehlen, M. (2005). Response of diatoms distribution to global warming and potential implications: A global model study. *Geophysical Research Letters*, *32*, L19606. https://doi.org/10.1029/2005GL023653

Boss, E., & Behrenfeld, M. (2010). In situ evaluation of the initiation of the North Atlantic phytoplankton bloom. *Geophysical Research Letters*, *37*, L18603. https://doi.org/10.1029/2010GL044174

Boyce, D. G., Lewis, M. R., & Worm, B. (2010). Global phytoplankton decline over the past century. *Nature*, *466*(7306), 591–596. https://doi.org/10.1038/nature09268

Boyd, P. W., & Doney, S. C. (2002). Modelling regional responses by marine pelagic ecosystems to global climate change. *Geophysical Research Letters*, *29*(16), 1806. https://doi.org/10.1029/2001GL014130

Brody, S. R., & Lozier, M. S. (2014). Changes in dominant mixing length scales as a driver of subpolar phytoplankton bloom initiation in the North Atlantic. *Geophysical Research Letters*, *41*, 3197–3203. https://doi.org/10.1002/2014GL059707

Brody, S. R., & Lozier, M. S. (2015). Characterizing upper-ocean mixing and its effect on the spring phytoplankton bloom with in situ data. *ICES Journal of Marine Science: Journal du Conseil*, *72*(6), 1961–1970. https://doi.org/10.1093/icesjms/fsv006

Cabre, A., Shields, D., Marinov, I., & Kostadinov, T. S. (2016). Phenology of size-partitioned phytoplankton carbon-biomass from ocean color remote sensing and CMIP5 models. *Frontiers in Marine Science*, *3*.

Capotondi, A., Alexander Michael, A., Bond Nicholas, A., Curchitser Enrique, N., & Scott James, D. (2012). Enhanced upper ocean stratification with climate change in the CMIP3 models. *Journal of Geophysical Research*, *117*, C04031. https://doi.org/10.1029/2011JC007409

Chavez, F. P., Strutton, P. G., & McPhaden, M. J. (1998). Biological-physical coupling in the central equatorial Pacific during the onset of the 1997–98 El Niño. *Geophysical Research Letters*, *25*(19), 3543–3546. https://doi.org/10.1029/98GL02729

Christian, J. R., Verschell, M. A., Murtugudde, R., Busalacchi, A. J., & McClain, C. R. (2001). Biogeochemical modelling of the tropical Pacific Ocean. I: Seasonal and interannual variability. *Deep Sea Research Part II: Topical Studies in Oceanography*, *49*(1–3), 509–543. http://doi.org/10.1016/S0967-0645(01)00110-2

Corno, G., Karl, D. M., Church, M. J., Letelier, R. M., Lukas, R., Bidigare, R. R., & Abbott, M. R. (2007). Impact of climate forcing on ecosystem processes in the North Pacific subtropical gyre. *Journal of Geophysical Research*, *112*, C04021. https://doi.org/10.1029/2006JC003730

Dave, A. C., & Lozier, M. S. (2010). Local stratification control of marine productivity in the subtropical North Pacific. *Journal of Geophysical Research*, *115*, C12032. https://doi.org/10.1029/2010JC006507

Dave, A. C., & Lozier, M. S. (2013). Examining the global record of interannual variability in stratification and marine productivity in the low-latitude and mid-latitude ocean. *Journal of Geophysical Research: Oceans*, *118*, 3114–3127. https://doi.org/10.1002/jgrc.20224

de Boyer Montégut, C., Madec, G., Fischer, A. S., Lazar, A., & Iudicone, D. (2004). Mixed layer depth over the global ocean: An examination of profile data and a profile-based climatology. *Journal of Geophysical Research*, *109*, C12003. https://doi.org/10.1029/2004JC002378

Doney, S. C., Fabry, V. J., Feely, R. A., & Kleypas, J. A. (2009). Ocean acidification: The other CO_2 problem. *Annual Review of Marine Science*, *1*(1), 169–192. https://doi.org/10.1146/annurev.marine.010908.163834.

Dufois, F., Hardman-Mountford, N. J., Greenwood, J., Richardson, A. J., Feng, M., & Matear, R. J. (2016). Anticyclonic eddies are more productive than cyclonic eddies in subtropical gyres because of winter mixing. *Science Advances*, *2*(5), e1600282. https://doi.org/10.1126/sciadv.1600282

Eppley, R. W., & Peterson, B. J. (1979). Particulate organic matter flux and planktonic new production in the deep ocean. *Nature*, *282*(5740), 677–680. https://doi.org/10.1038/282677a0

Field, C. B., Behrenfeld, M. J., Randerson, J. T., & Falkowski, P. (1998). Primary production of the biosphere: Integrating terrestrial and oceanic components. *Science*, *281*(5374), 237–240.

Gregg, W. W. (2005). Recent trends in global ocean chlorophyll. *Geophysical Research Letters*, *32*, L03606. https://doi.org/10.1029/2004GL021808

Gregg, W. W., Conkright, M. E., Ginoux, P., O'Reilly, J. E., & Casey, N. W. (2003). Ocean primary production and climate: Global decadal changes. *Geophysical Research Letters*, *30*(15), 1809. https://doi.org/10.1029/2003GL016889

Gregg, W. W., & Rousseaux, C. S. (2014). Decadal trends in global pelagic ocean chlorophyll: A new assessment integrating multiple satellites, in situ data, and models. *Journal of Geophysical Research: Oceans*, *119*, 5921–5933. https://doi.org/10.1002/2014JC010158

Gregg, W. W., Rousseaux, C. S., & Franz, B. A. (2017). Global trends in ocean phytoplankton: A new assessment using revised ocean colour data. *Remote Sensing Letters*, *8*(12), 1102–1111. https://doi.org/10.1080/2150704X.2017.1354263

Henson, S. A., Sarmiento, J. L., Dunne, J. P., Bopp, L., Lima, I., Doney, S. C., & Beaulieu, C. (2010). Detection of anthropogenic climate change in satellite records of ocean chlorophyll and productivity. *Biogeosciences*, *7*(2), 621–640. https://doi.org/10.5194/bg-7-621-2010

Iglesias-Rodriguez, M. D., Halloran, P. R., Rickaby, R. E. M., Hall, I. R., Colmenero-Hidalgo, E., Gittins, J. R., et al. (2008). Phytoplankton calcification in a high-CO_2 world. *Science*, *320*(5874), 336–340. https://doi.org/10.1126/science.1154122

Irwin, A. J., & Oliver, M. J. (2009). Are ocean deserts getting larger? *Geophysical Research Letters*, *36*, L18609. https://doi.org/10.1029/2009GL039883

Kostadinov, T. S., Cabré, A., Vedantham, H., Marinov, I., Bracher, A., Brewin, R. J. W., et al. (2017). Inter-comparison of phytoplankton functional type phenology metrics derived from ocean color algorithms and Earth system models. *Remote Sensing of Environment*, *190*, 162–177. http://doi.org/10.1016/j.rse.2016.11.014

Kostadinov, T. S., Milutinović, S., Marinov, I., & Cabré, A. (2016). Carbon-based phytoplankton size classes retrieved via ocean color estimates of the particle size distribution. *Ocean Science*, *12*(2), 561–575. https://doi.org/10.5194/os-12-561-2016

Kostadinov, T. S., Siegel, D. A., & Maritorena, S. (2009). Retrieval of the particle size distribution from satellite ocean color observations. *Journal of Geophysical Research*, *114*, C09015. https://doi.org/10.1029/2009JC005303

Kostadinov, T. S., Siegel, D. A., & Maritorena, S. (2010). Global variability of phytoplankton functional types from space: Assessment via the particle size distribution. *Biogeosciences*, *7*(10), 3239–3257. https://doi.org/10.5194/bg-7-3239-2010

Krumhardt, K. M., Lovenduski, N. S., Freeman, N. M., & Bates, N. R. (2016). Apparent increase in coccolithophore abundance in the subtropical North Atlantic from 1990 to 2014. *Biogeosciences*, *13*(4), 1163–1177. https://doi.org/10.5194/bg-13-1163-2016

Laws, E. A., & Bannister, T. T. (1980). Nutrient- and light-limited growth of *Thalassiosira fluviatilis* in continuous culture, with implications for phytoplankton growth in the ocean1. *Limnology and Oceanography*, *25*(3), 457–473. https://doi.org/10.4319/lo.1980.25.3.0457

Lehahn, Y., Koren, I., Sharoni, S., d'Ovidio, F., Vardi, A., & Boss, E. (2017). Dispersion/dilution enhances phytoplankton blooms in low-nutrient waters. *Nature Communications*, *8*, 14,868. https://doi.org/10.1038/ncomms14868

Lozier, M. S., Dave, A. C., Palter, J. B., Gerber, L. M., & Barber, R. T. (2011). On the relationship between stratification and primary productivity in the North Atlantic. *Geophysical Research Letters*, *38*, L18609. https://doi.org/10.1029/2011GL049414

Mackey, K. R. M., Morris, J. J., Morel, F. M. M., & Kranz, S. A. (2015). Response of photosynthesis to ocean acidification. *Oceanography*, *28*(2), 74–91. https://doi.org/10.5670/oceanog.2015.33

Martinez, E., Maamaatuaiahutapu, K., & Taillandier, V. (2009). Floating marine debris surface drift: Convergence and accumulation toward the South Pacific subtropical gyre. *Marine Pollution Bulletin*, *58*(9), 1347–1355. https://doi.org/10.1016/j.marpolbul.2009.04.022

McClain, C. R., Signorini, S. R., & Christian, J. R. (2004). Subtropical gyre variability observed by ocean-color satellites. *Deep Sea Research Part II: Topical Studies in Oceanography*, *51*, 281–301.

Paasche, E. (1998). Roles of nitrogen and phosphorus in coccolith formation in *Emiliania huxleyi* (Prymnesiophyceae). *European Journal of Phycology*, *33*(1), 33–42. https://doi.org/10.1080/09670269810001736513

Palter, J. B., Lozier, M. S., & Barber, R. T. (2005). The effect of advection on the nutrient reservoir in the North Atlantic subtropical gyre. *Nature*, *437*(7059), 687–692. https://doi.org/10.1038/nature03969, https://www.nature.com/articles/nature03969

Polovina, J. J., Dunne, J. P., Woodworth, P. A., & Howell, E. A. (2011). Projected expansion of the subtropical biome and contraction of the temperate and equatorial upwelling biomes in the North Pacific under global warming. *ICES Journal of Marine Science*, *68*(6), 986–995. https://doi.org/10.1093/icesjms/fsq198

Polovina, J. J., Howell, E. A., & Abecassis, M. (2008). Ocean's least productive waters are expanding. *Geophysical Research Letters*, *35*, L03618. https://doi.org/10.1029/2007GL031745

Radenac, M.-H., Léger, F., Singh, A., & Delcroix, T. (2012). Sea surface chlorophyll signature in the tropical Pacific during eastern and central Pacific ENSO events. *Journal of Geophysical Research*, *117*, C04007. https://doi.org/10.1029/2011JC007841

Radenac, M. H., Menkes, C., Vialard, J., Moulin, C., Dandonneau, Y., Delcroix, T., et al. (2001). Modeled and observed impacts of the 1997–1998 El Niño on nitrate and new production in the equatorial Pacific. *Journal of Geophysical Research*, *106*(C11), 26,879–26,898. https://doi.org/10.1029/2000JC000546

Rivero-Calle, S., Gnanadesikan, A., Del Castillo, C. E., Balch, W. M., & Guikema, S. D. (2015). Multidecadal increase in North Atlantic coccolithophores and the potential role of rising CO(2). *Science*, *350*(6267), 1533–1537. https://doi.org/10.1126/science.aaa8026

Rodríguez, F., Chauton, M., Johnsen, G., Andresen, K., Olsen, L. M., & Zapata, M. (2006). Photoacclimation in phytoplankton: Implications for biomass estimates, pigment functionality and chemotaxonomy. *Marine Biology*, *148*(5), 963–971. https://doi.org/10.1007/s00227-005-0138-7

Schluter, L., Lohbeck, K. T., Gutowska, M. A., Groger, J. P., Riebesell, U., & Reusch, T. B. H. (2014). Adaptation of a globally important coccolithophore to ocean warming and acidification. *Nature Climate Change*, *4*(11), 1024–1030. https://doi.org/10.1038/nclimate2379. http://www.nature.com/nclimate/journal/v4/n11/abs/nclimate2379.html

Siegel, D. A., Behrenfeld, M. J., Maritorena, S., McClain, C. R., Antoine, D., Bailey, S. W., & Yoder, J. A. (2013). Regional to global assessments of phytoplankton dynamics from the SeaWiFS mission. *Remote Sensing of Environment*, *135*, 77–91. https://doi.org/10.1016/j.rse.2013.03.025

Signorini, S. R., Franz, B. A., & McClain, C. R. (2015). Chlorophyll variability in the oligotrophic gyres: Mechanisms, seasonality and trends. *Frontiers in Marine Science*, *2*. https://doi.org/10.3389/fmars.2015.00001

Signorini, S. R., & McClain, C. R. (2012). Subtropical gyre variability as seen from satellites. *NASA Publications*, 193. http://digitalcommons.unl.edu/nasapub/193

Stone, L., Rajagopalan, B., Bhasin, H., & Loya, Y. (1999). Mass coral reef bleaching: A recent outcome of increased El Niño activity? *Ecology Letters*, *2*(5), 325–330. https://doi.org/10.1046/j.1461-0248.1999.00092.x

Strutton, P. G., & Chavez, F. P. (2000). Primary productivity in the equatorial Pacific during the 1997–1998 El Niño. *Journal of Geophysical Research*, *105*(C11), 26,089–26,101. https://doi.org/10.1029/1999JC000056

Turk, D., McPhaden, M. J., Busalacchi, A. J., & Lewis, M. R. (2001). Remotely sensed biological production in the equatorial Pacific. *Science*, *293*(5529), 471–474. https://doi.org/10.1126/science.1056449

Vantrepotte, V., & Mélin, F. (2011). Inter-annual variations in the SeaWiFS global chlorophyll *a* concentration (1997–2007). *Deep Sea Research Part I: Oceanographic Research Papers*, *58*(4), 429–441. https://doi.org/10.1016/j.dsr.2011.02.003

Volpe, G., Nardelli, B. B., Cipollini, P., Santoleri, R., & Robinson, I. S. (2012). Seasonal to interannual phytoplankton response to physical processes in the Mediterranean Sea from satellite observations. *Remote Sensing of Environment*, *117*, 223–235. https://doi.org/10.1016/j.rse.2011.09.020

Volpe, G., Santoleri, R., Vellucci, V., Ribera d'Alcalà, M., Marullo, S., & D'Ortenzio, F. (2007). The colour of the Mediterranean Sea: Global versus regional bio-optical algorithms evaluation and implication for satellite chlorophyll estimates. *Remote Sensing of Environment*, *107*(4), 625–638. https://doi.org/10.1016/j.rse.2006.10.017

Weber, T. S., & Deutsch, C. (2010). Ocean nutrient ratios governed by plankton biogeography. *Nature*, *467*(7315), 550–554. https://doi.org/10.1038/nature09403, https://www.nature.com/articles/nature09403#supplementary-information

Wernand, M. R., van der Woerd, H. J., & Gieskes, W. W. (2013). Trends in ocean colour and chlorophyll concentration from 1889 to 2000, worldwide. *PLoS ONE*, *8*(6), e63766. https://doi.org/10.1371/journal.pone.0063766

Westberry, T. K., Schultz, P., Behrenfeld, M. J., Dunne, J. P., Hiscock, M. R., Maritorena, S., & Siegel, D. A. (2016). Annual cycles of phytoplankton biomass in the subarctic Atlantic and Pacific Ocean. *Global Biogeochemical Cycles*, *30*, 175–190. https://doi.org/10.1002/2015GB005276

References From the Supporting Information

Carton, J. A., Chepurin, G., & Cao, X. (2000). A simple ocean data assimilation analysis of the global Upper Ocean 1950–95. Part II: Results. *Journal of Physical Oceanography*, *30*(2), 311–326. https://doi.org/10.1175/1520-0485(2000)030<0311:ASODAA>2.0.CO;2

Carton, J. A., & Giese, B. S. (2008). A reanalysis of ocean climate using simple ocean data assimilation (SODA). *Monthly Weather Review*, *136*(8), 2999–3017. https://doi.org/10.1175/2007mwr1978.1

Menden-Deuer, S., & Lessard, E. J. (2000). Carbon to volume relationships for dinoflagellates, diatoms, and other protist plankton. *Limnology and Oceanography*, *45*(3), 569–579. https://doi.org/10.4319/lo.2000.45.3.0569

Racault, M. F., Sathyendranath, S., Menon, N., & Platt, T. (2016). Phenological responses to ENSO in the global oceans. *Surveys in Geophysics*, *38*(1), 277–293. https://doi.org/10.1007/s10712-016-9391-1

Takahashi, T., Sutherland, S. C., Wanninkhof, R., Sweeney, C., Feely, R. A., Chipman, D. W., et al. (2009). Climatological mean and decadal change in surface ocean pCO_2, and net sea–air CO_2 flux over the global oceans. *Deep Sea Research Part II: Topical Studies in Oceanography*, *56*(8-10), 554–577. https://doi.org/10.1016/j.dsr2.2008.12.009

Wolter, K., & M. S. Timlin, (1993). Monitoring ENSO in COADS with a seasonally adjusted principal component index. Proc. of the 17th climate diagnostics workshop, Norman, OK, NOAA/N MC/CAC, NSSL, Oklahoma Clim. Survey, CIMMS and the School of Meteor., University of Oklahoma, 52-57.